Published online 31 May 2017

Nucleic Acids Research, 2017, Vol. 45, No. 14 ***8551–8563***
doi: 10.1093/nar/gkx481

DRB4 dsRBD1 drives dsRNA recognition in *Arabidopsis thaliana* tasi/siRNA pathway

Sai Chaitanya Chiliveri[1], Ramdas Aute[1], Upasana Rai[1,2] and Mandar V. Deshmukh[1,2,*]

[1]CSIR-Centre for Cellular and Molecular Biology, Uppal Road, Hyderabad 500007, India and [2]Academy of Scientific and Innovative Research (AcSIR), CSIR – Centre for Cellular and Molecular Biology, Uppal Road, Hyderabad 500007, India

Received December 18, 2016; Revised April 26, 2017; Editorial Decision May 15, 2017; Accepted May 17, 2017

ABSTRACT

In *Arabidopsis thaliana*, endogenous *trans*-acting and exogenous siRNA pathways are initiated by the interaction of DRB4 with trigger dsRNA. Further, DCL4:DRB4 complex cleaves the dsRNA into 21 bp siRNA. Understanding molecular determinants and mechanistic details of dsRNA recognition by DRB4 is vital for inducing long-term RNAi-mediated gene regulation in plants. Here, we present solution structures of individual and concatenated DRB4 dsRBDs and demonstrate modes of dsRNA binding by employing NMR, ITC and site-specific mutagenesis. While both dsRBDs adopt the canonical α−β−β−β−α fold, key structural differences and ms-μs dynamics located at the RNA binding region were observed for dsRBD1. These features favor dsRBD1 to orient itself and make stronger tripartite contact with dsRNA, a feature missing in dsRBD2. Additionally, the inter-domain orientation induced by the linker restricts the mobility of dsRBD2, resulting in the steric hindrance of α1 helix in dsRBD2, and leads in further reduction of its dsRNA binding activity. Our study deciphers functional roles of DRB4 domains by showing that dsRBD1 drives the tasiRNA/siRNA pathway. Furthermore, we identify a potential role of the C-terminal region of DRB4 in protein:protein interaction as it possesses six PxxP motifs, binds to Zn^{2+} and contains a small structural domain.

INTRODUCTION

In *Arabidopsis*, small RNA mediated gene regulation is performed by four Dicer-like enzymes (DCLs; DCL1-4) and five partner dsRNA binding proteins (dsRBPs; DRB1-5) which act independently in response to a variety of precursor dsRNA of diverse origin and structures (1). Despite high sequence similarities and identical domain architectures, the functional roles of DCLs and their partner dsRBPs are well defined which impart high level of specificity to the plant small RNA induced gene regulation and silencing mechanism (2–5).

Among these, DCL4 together with DRB4 facilitates both *trans*-acting (*tasi*RNA) and viral siRNA (siRNA) pathways (6–10). Genetic and biochemical studies established that DRB4 mostly interacts with DCL4 and localizes in the nucleus, although, a fraction of DRB4 has been observed to be either free or associated with other proteins (1,11,12). DCL4 (*dcl4-2*) and DRB4 (*drb4-1*) mutants manifest similar phenotype of downwardly curled rosette leaves and anthocyanin over-accumulation. Crude extracts from *dcl4-2* and *drb4-1* plants could not cleave dsRNA, whereas *drb4-1* extract supplemented with recombinant DRB4 resulted in dsRNA cleavage, signifying that both DCL4 and DRB4 are inter-dependent for RNAi functioning in plants (13). However, unlike HYL1, DRB4 is not involved in guide strand selection (14). Additionally, DCL4-DUF283 and sDCL4 were shown to interact with DRB4 dsRBD1 and dsRBD2, respectively, and the dsRNA binding residues (H32 and K133) were found to participate in DCL4 binding (13,15). Nonetheless, in canonical dsRBDs conserved H and K mediate dsRNA recognition and not Dicer binding.

In parallel to RNAi, DRB4 is involved in resistance (R) gene-mediated or species-specific immunity, which is induced by the association of a strain-specific avirulence (*avr*) protein from pathogen with a cognate plant R protein (16). The R protein, HRT [Hypersensitive response (HR) to *Turnip crinkle virus* (TCV)], in *Arabidopsis* is activated upon recognition of the TCV coat protein (CP), which is a potent suppressor of RNAi. TCV infection increases DRB4′s cytosolic fraction, which is required for the stability of HRT (17,18). In addition, the viral translational transactivator protein P6, from *Cauliflower mosaic virus* (CaMV), immunoprecipitates with DRB4 and delineates its activity (19). Similarly, increase in DRB4′s cytoplasmic pool was observed with *Turnip yellow mosaic virus* (TYMV) infection, where DRB4 dsRBD2 directly interacts with TYMV RNA translational enhancer, which adopts tRNA like structure (20). Moreover, DRB7.1 and DRB7.2

*To whom correspondence should be addressed. Tel: +91 40 2719 2646; Email: mvdesh@ccmb.res.in

independently interact with DRB4 to attenuate the siRNA production as well as sequester endoIR siRNA, respectively (21,22).

DRB4 consists of multiple dsRNA binding domains (dsRBDs) that are highly conserved with its homologues, such as, DRB1 (*A. thaliana*), TRBP (*H. sapiens*), RDE-4 (*C. elegans*), and R2D2 (*D. melanogaster*) etc. A canonical dsRBD is comprised of α1–β1–β2–β3–α2 structure where two α helices organize to form an α1–α2 interface that packs against antiparallel β sheet formed by β1−β2−β3 (23). dsRBDs recognize dsRNA in a sequence-independent manner, through the helical face in which residues Q/H and E in α1 contact minor groove, KKxxK motif of α2 N-terminus binds to the adjacent major groove, and the H of the β1−β2 loop contacts subsequent minor groove (24). In DRB4, the linker connecting tandem dsRBDs spans nine amino acids, making it the shortest among the known dsRBPs. Further, DRB4 possesses a long C-terminal region of about 200 amino acids, which does not show any sequence homology with known proteins.

Despite available information, structural and molecular basis of DRB4′s involvement in two independent pathways remain elusive. Moreover, functional annotation of DRB4 domains responsible for diverse activities may eventually allow its exploitation for favorable gene silencing. In this study, we present structural and biochemical characterization of DRB4. The favorable structural and conformational flexibility intrinsic to dsRBD1 imparts advantages to dsRBD1 in dsRNA recognition over dsRBD2. Additionally, we show that DRB4 dsRBDs adopt a preferred orientation in which steric hindrance induced by the linker limits dsRBD2′s accessibility to dsRNA. Further, investigations on DRB4 C-terminal region led to a few novel findings, such as identification of several PxxP motifs, a structured domain, and zinc binding ability, suggesting its possible role in protein-protein interactions. Altogether, we propose a functional DRB4 model to suggest important roles of individual structural motifs in RNAi.

MATERIALS AND METHODS

Cloning, expression and purification

DRB4 and its domains were cloned and expressed in *Escherichia coli* as described earlier (25). All constructs mentioned in the study were initially purified by affinity chromatography (His_6 tag) and followed by size exclusion chromatography using either G75 or G200 Sepharose preparative columns. Details of cloning, expression and purification are described in supplementary materials and methods.

Gel shift assay

Eighty nucleotide long sense and antisense RNA were internally labeled with [α-^{32}P]CTP using T7 megashortscript kit (Ambion) and gel purified. For gel mobility shift assays, recombinant proteins (final concentration ∼ 0.1–10 μM) were incubated with the [α-^{32}P] labeled RNA (final concentration ∼ 200 pM) for 1 h at 4°C in dsRNA buffer (20 mM HEPES (pH 7.2), 100 mM NaCl and 2 mM DTT). Samples were separated on a 15% native PAGE and analyzed using autoradiography. The protein:dsRNA complexes were quantified by measuring the amount of radioactivity shown by free dsRNA divided by the total amount of radioactivity (fraction bound = 1 – [$dsRNA_{free}/dsRNA_{total}$]).

NMR derived restraints, structure calculation and ^{15}N CPMG

All NMR spectra were collected at 298 K on a Bruker Avance II 600 MHz or Avance III 700 MHz spectrometer, equipped with a triple resonance TCI cryoprobe. Backbone and sidechain chemical shifts for DRB4D1D2 were adopted from BMRB accession no. 25138 (25). Distance restraints were derived using 3D ^{15}N/^{13}C NOESY HSQC experiments. ^{15}N–^{1}H residual dipolar couplings were obtained by externally aligning DRB4D1D2 in Pf1 phages. Long-range distance restraints were achieved from intensity drop in the amide resonances under paramagnetic environment, created by MTSL. ^{15}N–{^{1}H} heteronuclear NOE experiments on DRB4D1D2 and DRB4C were performed at 600 MHz spectrometer and data was subjected to standard analysis. Additionally, ^{15}N CPMG was performed on DRB4D1 and DRB4D2 at 600 and 700 MHz spectrometers and the data was analyzed using CPMGFit. Additional information on this section and backbone chemical shift assignments of DRB4C is detailed in supplementary materials and methods.

NMR based binding studies

[U-^{15}N] 100 μM various DRB4 constructs, such as DRB4D1D2, DRB4D2D1, DRB4D1 and DRB4D2 (in 20 mM HEPES (pH 7.2), 100 mM NaCl and 2 mM DTT), were titrated against 13 bp and 20 bp dsRNA with increasing concentrations in the range of 0–200 μM. Perturbations in the chemical shifts observed in ^{1}H–^{15}N HSQC were estimated using Equation (1) as:

$$\Delta\delta = \sqrt{(\Delta H)^2 + \left(\frac{\Delta N}{7}\right)^2} \quad (1)$$

Isothermal titration calorimetry

Isothermal titration calorimetric (ITC) measurements were performed at 25°C using Microcal ITC-200. Protein and RNA samples were buffer exchanged in 20 mM HEPES (pH 7.2), 100 mM NaCl and 2 mM DTT. For shorter dsRNA, 20 bp dsRNA (200 μM) was injected into the cell containing 20–30 μM of DRB4D1D2, DRB4D2D1, DRB4D1 and DRB4D2. For 80 bp dsRNA, 80–100 μM of DRB4, DRB4D1D2, DRB4D2D1, DRB4D1, DRB4D2 and DRB4D2C were titrated with 2 μM dsRNA which was placed in the cell. For AtDCL4-DUF283 interaction with DRB4, DRB4D1D2 (180 μM) was injected into the cell containing AtDCL4-DUF283 (45 μM). For Zn^{2+} interaction, 2 mM of $ZnCl_2$ was injected into the cell containing 50 μM DRB4D1D2 or DRB4C. After performing baseline integration of the spectra, thermodynamic analysis was achieved by fitting curves to one or two sets of identical site model.

RESULTS

Domains of DRB4 are independent structural units in solution

We designed, cloned, heterologously over-expressed and purified various constructs of DRB4 (i.e. DRB4, DRB4D1D2, DRB4D1, DRB4D2, DRB4D2D1, DRB4C and DRB4Cc) (Figure 1A). ^{1}H–^{15}N TROSY-HSQC spectrum of DRB4 is highly superimposable with DRB4D1D2 and DRB4C (Supplementary Figure S1A). Also, ^{1}H–^{15}N HSQCs of DRB4D1 and DRB4D2 are superimposable with DRB4D1D2 (Supplementary Figure S1B and D). Chemical shift deviations in the amide resonances ($\Delta\delta$) of DRB4D1D2 with corresponding peaks in DRB4 show insignificant changes and strongly suggest that the DRB4D1D2 and C-terminus do not interact with each other (Supplementary Figure S1C).

Primary sequence analysis of DRB4C neither predicted any conserved domain nor showed any homology with a known protein except the six PxxP motifs that are interspersed at even intervals (Figure 1A). The ^{1}H–^{15}N HSQC confirmed that most of the DRB4C is disordered in solution as we observed narrow spectral dispersion in the proton dimension (Supplementary Figure S1E). The random coil nature of DRB4C was also evident from the chemical shifts of Cα and Cβ. Moreover, the majority of DRB4C resonances assume a negative value in ^{15}N–$\{^{1}H\}$ hetronuclear NOE corroborating its unstructured nature (Figure 1B). Interestingly, resonances belonging to residues 294–355 (i.e. DRB4Cc) were absent in the ^{1}H–^{15}N HSQC of DRB4C. Protein disorder algorithms (26) predicted that DRB4Cc may assume an ordered conformation. Subsequently, a well-dispersed ^{1}H–^{15}N HSQC for DRB4Cc implied the presence of a tertiary structure (Supplementary Figure S1F). The broadening of resonances beyond detection of DRB4Cc in the ^{1}H–^{15}N HSQC of DRB4C is surprising, nonetheless, we postulate that the drag created by ∼150 long unstructured amino acids of DRB4C on the small structured DRB4Cc causes artificial enhancement in its τ_c. The functional significance of DRB4Cc can be deciphered only by *de novo* structure determination. Collectively, these results indicate that individual dsRBDs and C-terminal region behave as independent structural units in solution.

Functional characterization of DRB4 domains

To identify the functional dsRNA binding domains in DRB4, we performed electrophoretic mobility shift assays (EMSA) with the aforementioned constructs (Figure 1C). As expected, DRB4, DRB4D1D2, DRB4D1, DRB4D2, and DRB4D2D1, which contain one or more predicted dsRBD, showed prominent gel shifts arising due to their binding to 80 bp dsRNA, whereas, no mobility shift was observed with DRB4C.

DRB4C behaves as a stable monomer at various concentrations and (Supplementary Figure S2A) titration of DRB4C with guanidine hydrochloride (GuHCl) resulted in uniform and narrow ^{15}N line widths for all resonances, indicating that the residual structure present in the native form of DRB4C is completely lost (Supplementary Figure S2B). We evaluated zinc binding ability of DRB4C as it contains multiple Cys and as ZincExplorer (24) server predicted high Zn^{2+} coordination probability for C280, C298 and C325. Indeed, ITC showed that DRB4C binds to $ZnCl_2$ with a K_d of 23.6 μM (Figure 1D). At saturated concentrations of $ZnCl_2$, significant broadening for resonances located primarily at the C-terminus of DRB4C was observed in ^{1}H–^{15}N TROSY-HSQC (Figure 1E and Supplementary Figure S3A). Interestingly, DRB4D1D2 did not bind to Zn^{2+}, suggesting the Zn^{2+} binding specificity originates only from DRB4C (Supplementary Figure S3B). While zinc-binding proteins are known to also bind DNA or RNA, DRB4C did not bind to any dsRNA or dsDNA in the presence or absence of Zn^{2+} (Supplementary Figure S3C).

Altogether, the data suggests that the dsRNA binding activity of DRB4 exclusively stems from dsRBD regions and DRB4C may be necessary for additional activities such as Zn^{2+} binding as well as protein:protein interactions.

Solution structure of DRB4 dsRBDs

Sequence comparison with known dsRBPs revealed that DRB4 dsRBDs possess conserved dsRNA binding regions (Figure 2A). Pairwise sequence alignment for DRB4D1 and DRB4D2 shows 43% identity and 51% similarity.

Solution structures of individual domains displayed dsRBD fold, with residues 4–72 and 82–150 of DRB4D1 and DRB4D2, respectively, adopting α1–β1–β2–β3–α2 fold (Figure 2B and C). The linker region composed of residues 73–81 assumes random structure and does not make any contact with itself or rest of the structure. Ensemble structures of DRB4D1 and DRB4D2 converged with a backbone RMSD of 0.5 and 0.6Å, and heavy chain RMSD of 1.3 and 1.1 Å, respectively (Figure 2B and C and Table 1). Both domains demonstrated a contiguous positive charge at the interface formed by α1, β1–β2 loop and N-terminus of α2, indicating a potential dsRNA binding recognition surface (Supplementary Figure S4A and B).

Both dsRBDs (DRB4D1 and DRB4D2) are identical with 1.5 Å backbone RMSD (Figure 2D). The structural alignment shows that α1 in DRB4D2 is displaced by one helical turn with respect to DRB4D1. While, β1–β2 loop in both domains adopt flexible conformations, the loop in DRB4D1 is more inclined toward the helical face. DRB4D1 is more identical to HYL1 and TRBP (backbone RMSD 0.8 and 1.8 Å, respectively) (Figure 2E, Supplementary Figure S4C and D). Additionally, dsRNA recognition sites in DRB4D2 are deviated at α1 and N-terminus of α2 (backbone RMSD 1.5 and 2.1 Å, respectively).

Both DRB4 dsRBDs independently bind to dsRNA

To further explore the functional significance of subtle differences in the putative dsRNA recognition sites of DRB4D1 and DRB4D2, we performed titrations with different dsRNAs of varied lengths.

Normally, a minimum of 10–12 bp dsRNA is necessary and sufficient for a dsRBD to make tripartite contact with dsRNA (24,27). Naturally occurring regulatory dsRNA are often longer (>19 bp with 2nt 3′ overhang). In our experience, dsRNA longer than ∼20 bp results in the broadening of resonances in NMR based binding assays, therefore, we performed the assays using 13 bp and 20 bp dsRNA.

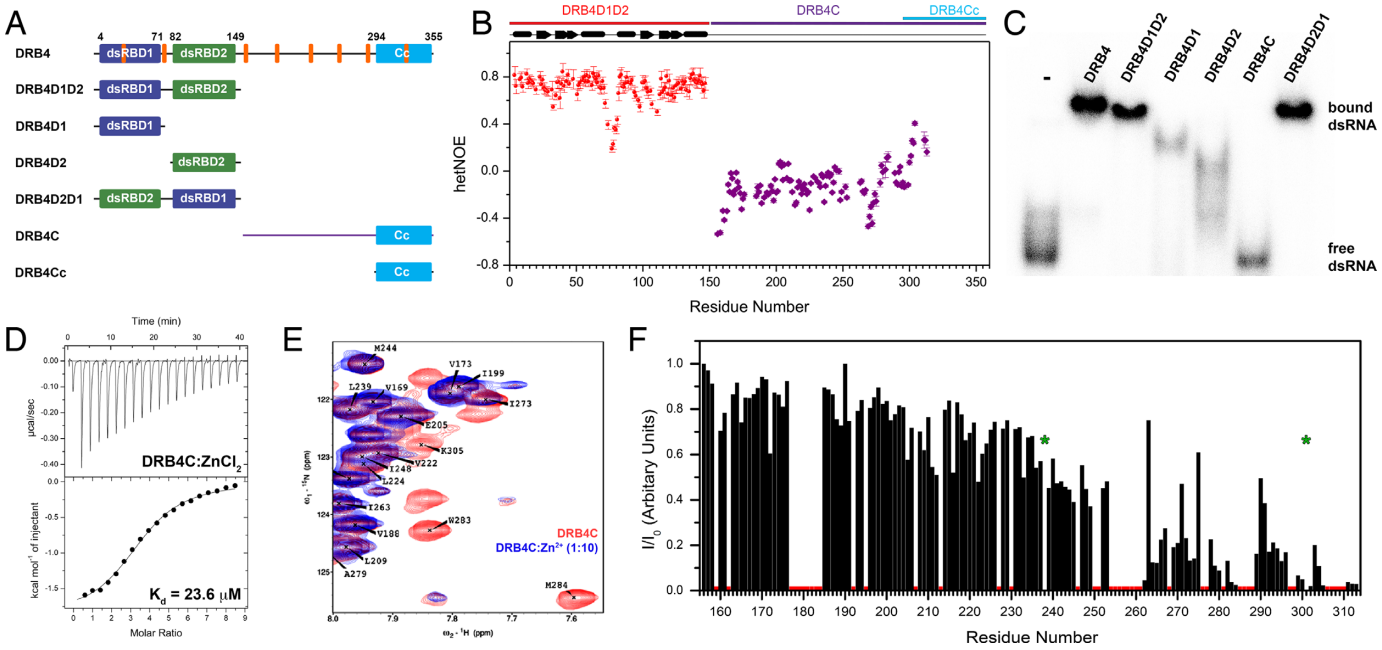

Figure 1. Domain architecture and functional characterization of DRB4 domains. (**A**) Various constructs of DRB4 used in the study are represented as: dsRBD1 (blue), dsRBD2 (green) and domain of unidentified function in the C-terminus (cyan). Orange segments in DRB4 denote PxxP motifs which may mediate protein:protein interactions. (**B**) ^{15}N–{^{1}H} heteronuclear NOE of DRB4 constructs suggesting that DRB4D1D2 possesses rigid structure, whereas, DRB4C is flexible. Since the majority of resonances belonging to DRB4Cc are broadened beyond detection, we could not estimate its rigidity, however, positive hetNOE for the N-terminal residues of DRB4Cc indicates that DRB4Cc may be structured. (**C**) Gel shift assay of 80 bp dsRNA with various DRB4 constructs. C-terminus lacking potential dsRBD fold does not bind to dsRNA, whereas other constructs bind to dsRNA. (**D**) ITC binding isotherm reveals Zn^{2+} binding exhibited by DRB4C. One set of identical binding sites to the integrated raw data yielded $K_d = 23.6 \pm 1.8$ μM ($N \approx 3$). (**E**) Excerpt of ^{1}H–^{15}N TROSY-HSQC of DRB4C upon titration with 10-fold molar excess $ZnCl_2$ displaying broadening of several resonances. (**F**) Normalized intensity ratios of DRB4C residues in the presence of Zn^{2+}. The decreased intensity ratios allowed mapping of binding interaction of Zn^{2+} with the C-terminal region of DRB4C. Residues A238 and D301 are broadened beyond detection and marked with green asterisks. Unassigned residues are marked with red bars.

Table 1. Structural statistics for dsRNA binding domains of DRB4

	DRB4D1	DRB4D2	DRB4D1D2
NOE	625	646	1292
Intraresidue	206	207	422
Sequential	187	164	361
Medium range [(i-j) ≤ 4]	76	115	193
Long range [(i-j) ≥ 4]	156	160	316
Hydrogen bonds	64	62	126
Dihedral angle restraints	136	135	273
NH RDC restraints	47	55	109
Q_{saupe} N-H$^{N\#}$	0.08	0.03	0.06
PRE			355
Number of distance restraints > 0.5 Å	0	0	0.3
Maximum amount of violation (Å)			0.6
Number of dihedral angle restraints > 5°	1.4	0.3	3.7
Maximum amount of violation (°)	7.2	6.5	8.5
Deviations from idealized geometry			
Bond lengths (Å)	0.004	0.003	0.003
Bond angles (°)	0.502	0.429	0.473
Impropers (°)	0.427	0.371	0.460
Average pairwise RMSD (Å)*			
Backbone atoms	0.5	0.6	0.9
Heavy atoms	1.33	1.14	1.5
Ramachandran statistics (%)*			
Most favored	90.3	87.3	88.7
Additionally allowed	9.7	12.7	10.5
Generously allowed	0	0	0.8
Disallowed	0	0	0

#Q_{saupe} derived for N–H^{N} using software PALES. The weightage on RDCs were ramped from 0.0 to 1.0. Calculations without RDCs or low RDC weightage did not affect the structure quality as estimated from Ramachandran statistics.
*for residues 3–71 and 82–150.

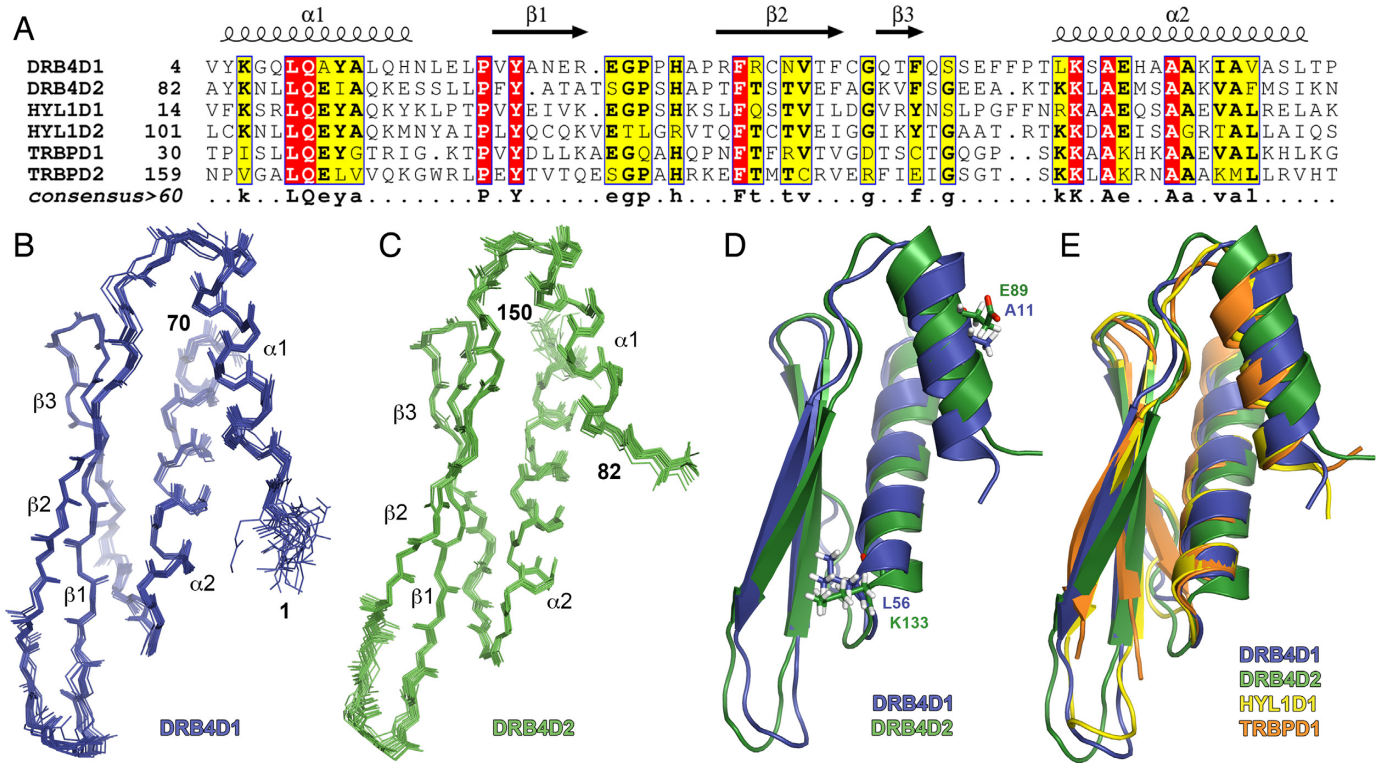

Figure 2. Solution structure of DRB4 dsRBDs. (**A**) Multiple sequence alignment of DRB4 dsRBDs with homologous proteins, HYL1 (*A. thaliana*) and TRBP (*H. sapiens*). Secondary structural elements from DRB4D1 are represented at the top of the alignment. Invariant amino acids are highlighted in red and those conserved by >60% are highlighted in yellow. Twenty lowest energy ensemble structures of (**B**) DRB4D1 and (**C**) DRB4D2. (**D**) Structural alignment of DRB4D1 with DRB4D2 showing differences in orientation at α1, N-terminus of α2 and β1−β2 loop. Residues involved in dsRNA binding which are different in both domains are annotated. (**E**) Structure comparison of DRB4D1 and DRB4D2, with HYL1D1 (PDB ID: 3ADG) and TRBPD1 (PDB ID: 3LLH) reveals that DRB4D1 is structurally more similar to its homologous dsRBDs.

The imino protons of 13 bp dsRNA were assigned using 2D NOESY and the assignments were traced after its titration with DRB4 domains (Supplementary Figure S5). The minor shifts observed in imino protons of U'10, U6 and the peak annotated with an asterisk may arise as there is a subtle sequence heterogeneity in key dsRNA binding residues between DRB4D1 and DRB4D2 (Figure 2D). Interestingly, the 1D ^{1}H NMR of the imino region of 20 bp dsRNA upon titration with DRB4D1, DRB4D2 and DRB4D1D2 shows significant broadening at ratios upto molar equivalence (Supplementary Figure S6). Changes in the amide environment were recorded for individual and tandemly connected domains in the presence of both types of dsRNA (Figure 3A, D, Supplementary Figures S7A, B, S9 and S10).

For 13 bp dsRNA, residues in α1, β1–β2 loop and N-terminus of α2 displayed significant Δδ for both DRB4D1 and DRB4D2 (Figure 3B and E). The resonances for V4, Y5, K6, L56 and K57 in DRB4D1 specifically showed broadening at substoichiometric concentrations and did not reappear even at the saturating concentration of dsRNA. Importantly, DRB4D1 recognizes dsRNA at intermediate time-scale (ms-μs) while DRB4D2 interacts with dsRNA at fast time-scale (ns), suggesting that DRB4D1 possesses a relatively better binding mode with dsRNA. Moreover, β1-β2 loop in DRB4D2, which is required to make a crucial contact with the minor groove of dsRNA, displayed lower magnitudes of Δδ. Nevertheless, the interface formed by α1, β1–β2 loop and N-terminus of α2 depicts contiguous dsRNA binding surface on both domains which is in agreement with the surface charge distribution plots (Figure 3G and H).

Interestingly, when 20 bp dsRNA was used as a substrate, residues in dsRNA binding regions of DRB4D1 underwent severe broadening (Supplementary Figure S7A and C), suggesting that the formation of DRB4D1:dsRNA complex exhibits kinetics at an intermediate time scale and may slide (or diffuse) over the dsRNA length as shown earlier for TRBP (28). An increased Δδ was observed for DRB4D2:20 bp dsRNA binding (Supplementary Figure S7B and D). The broadening of resonances for DRB4D1 but not for DRB4D2 motivated us to explore the binding modes of both DRB4D1 and DRB4D2 with 20 bp dsRNA using ITC (Figure 3C, F, Supplementary Figure S8A and B). Studies reveal that DRB4D1 recognizes 20 bp dsRNA using a two site binding mode yielding K_d of 0.3 μM and 2.7 μM, whereas DRB4D2 binds to 20 bp dsRNA with 1.0 μM affinity (Supplementary Table S1). Moreover, both domains show a stoichiometry of ∼0.25:1 suggesting that a single dsRNA molecule can be accessed by up to four individual dsRBDs (Supplementary Table S1). The stoichiometry obtained for DRB4 dsRBDs is in well agreement with TRBP dsRBDs (29). The two site binding mode derived from ITC and resonance broadening in NMR titrations suggest that

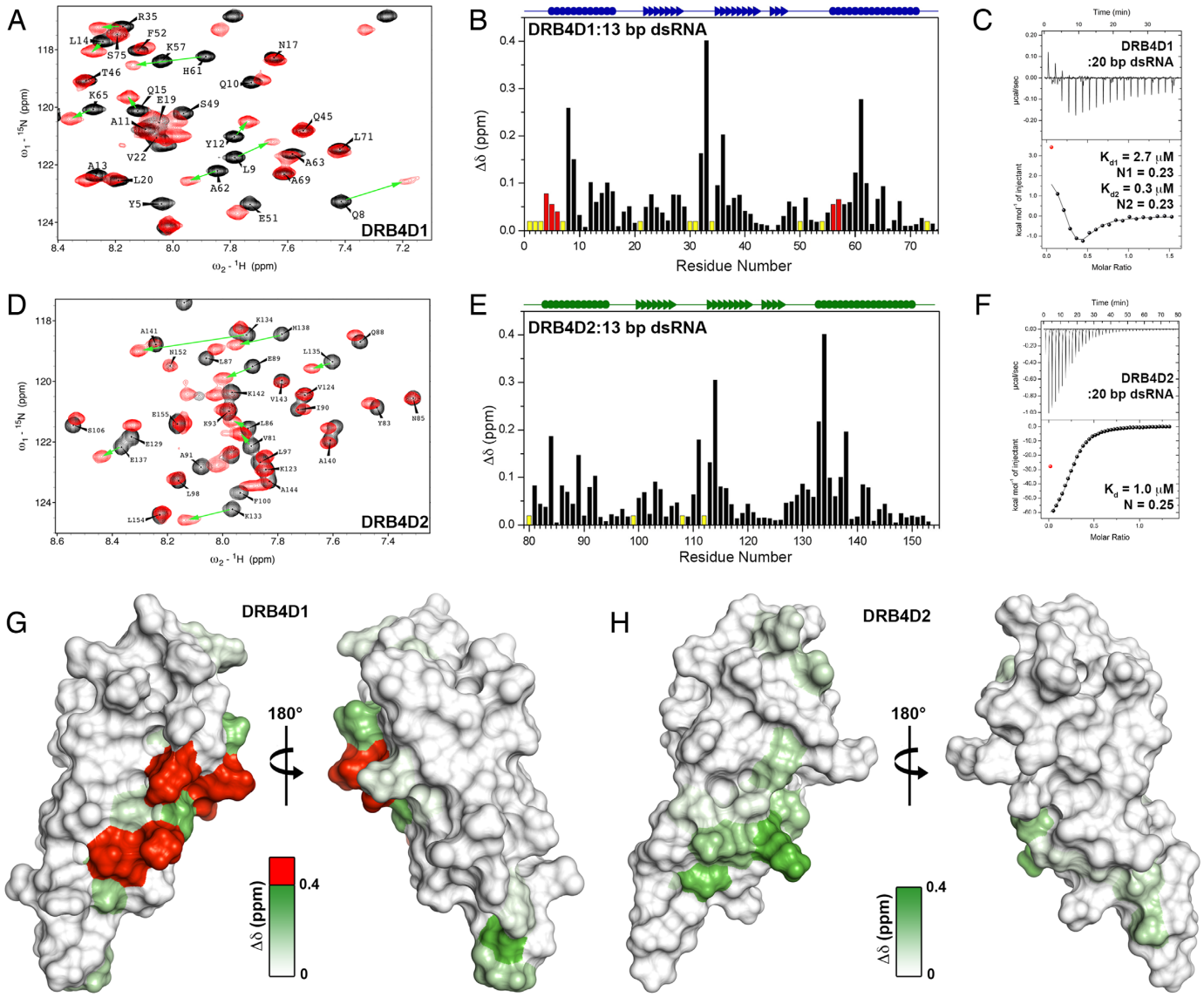

Figure 3. dsRNA binding studies of DRB4D1 and DRB4D2. ^{1}H–^{15}N HSQC excerpts of titration of DRB4D1 (**A**) and DRB4D2 (**D**) with 13 bp dsRNA. Resonances in black and red represent 1:0 and 1:2 molar equivalence of protein to dsRNA, respectively. Normalized chemical shift changes induced on DRB4D1 (**B**) and DRB4D2 (**E**) with 13 bp dsRNA, respectively. Residues that undergo severe broadening are shown in red whereas unassigned residues and prolines are color coded in yellow. Binding isotherms of DRB4D1 **(C)** and DRB4D2 (**F**) with 20 bp dsRNA, respectively. Upper panels show raw titration data, whereas, integrated injection enthalpy per mol of injectant is plotted in the lower panel, which is a function of the ratio of protein to dsRNA molar concentrations. For DRB4D1, the data was fitted to two-site sequential binding model and dissociation constant (K_d) estimated were 2.7±0.7 μM and 0.3±0.2 μM. Dissociation constant of 1.0±0.04 μM was observed for DRB4D2 with one-site binding mode. Surface plots representing dsRNA binding residues from DRB4D1 (**G**) and DRB4D2 (**H**). Color gradient from white to green signifies the extent of binding to dsRNA and residues that undergo broadening are represented in red. Data points colored in red in ITC graphs were not used for fitting and analysis.

DRB4D1 is probably better equipped to recognize longer dsRNA than DRB4D2.

DRB4 dsRBD1 drives dsRNA interaction

The different binding modes exhibited by DRB4 dsRBDs was quite unexpected and might not arise only from subtle structural differences. Therefore, we probed motions occurring at intermediate-slow timescale (ms–μs).

The analysis of ^{15}N CPMG data shows significant ms-μs motions for several residues in α1 of DRB4D1 (V4 and A13-N17) as observed from R_2 dispersion curves, yielding R_{ex} values in the range of 2.2–11 s^{-1} (Figure 4A). The intermediate timescale motions signify conformational flexibility required for α1 in dsRBD1 to properly position onto the minor groove of dsRNA (Figure 4B). Additionally, the broadening of amide resonance belonging to G7 due to solvent exchange did not allow measurement of ms-μs motions. Importantly, almost all residues in dsRBD2 show a flat R_2 dispersion curve suggesting the absence of motions at intermediate exchange regime (Figure 4C). As the active site residues in α1 (Q10 and E11) are hydrogen bonded to α1 C-terminus, the dynamics exhibited by dsRBD1 facili-

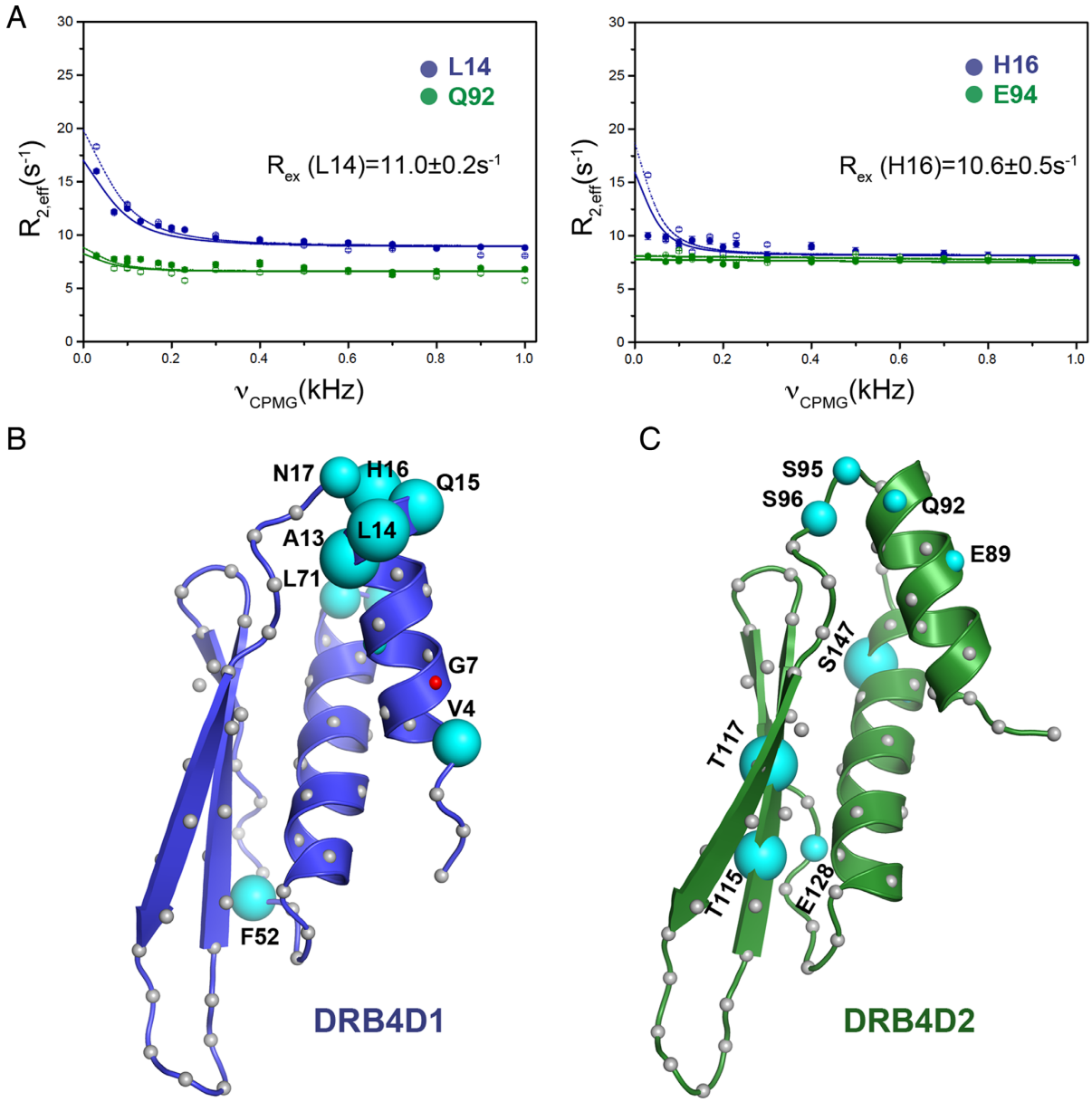

Figure 4. ^{15}N relaxation dispersion of DRB4D1 and DRB4D2. (**A**) Representative R_2 dispersion curves for residues in α1 (L14 and H16) of dsRBD1 and the corresponding residues in dsRBD2 (Q92 and E94). The simulated curves were fitted to raw data (in circles). Residues in α1 (L14 and H16: blue circles) of dsRBD1 show significant R_{ex}, whereas dsRBD2 residues (Q92 and E94: green circles) show flat dispersion curves, signifying ms-μs motions in dsRBD1. Data from 600 MHz and 700 MHz are shown as filled and hollow circles, respectively. (**B**) The exchange rates are represented as a function of sphere diameter for residues undergoing significant R_{ex}. Majority of residues exhibiting exchange are located on α1 of DRB4D1. R_{ex} shown by residues F52, L71 and T72 has no functional significance. (**C**) In DRB4D2, residues T115, T117 and S147 show R_{ex} without any functional significance.

tates appropriate dsRNA binding, which explains two site binding mode of dsRBD1 over dsRBD2.

We further investigated the dsRNA interaction with DRB4D1D2 to understand the role of individual domains when connected in tandem. For 13 bp dsRNA, several DRB4D1D2 residues show significant perturbations (Figure 5A). Normalized Δδ for dsRBD1 residues were identical to DRB4D1, whereas, a marked reduction in Δδ values were observed in dsRBD2 (Figures 5B, 3B and E). The data suggests that even at saturated dsRNA concentrations, about 70% of dsRBD2 remains inaccessible to dsRNA in the presence of dsRBD1. The titration of 20 bp dsRNA with DRB4D1D2 yielded ITC isotherm which was fitted using two site binding mode and exhibited K_d of 0.2 and 7.0 μM, identical to DRB4D1 (Figure 5C, Supplementary Figure S8C and Supplementary Table S1). The similarity in the binding modes between DRB4D1D2 and DRB4D1 suggests that the dsRBD1 plays the primary role in dsRNA recognition in DRB4. Additional ITC data where DRB4D1D2 was titrated against 20 bp dsRNA showed a single site binding mode resulting from averaged states (Supplementary Figure S8). The complex of DRB4D1D2:20 bp dsRNA yielded a stoichiometry of ∼ 0.25:1 (or 1:4 i.e. a single dsRNA molecule

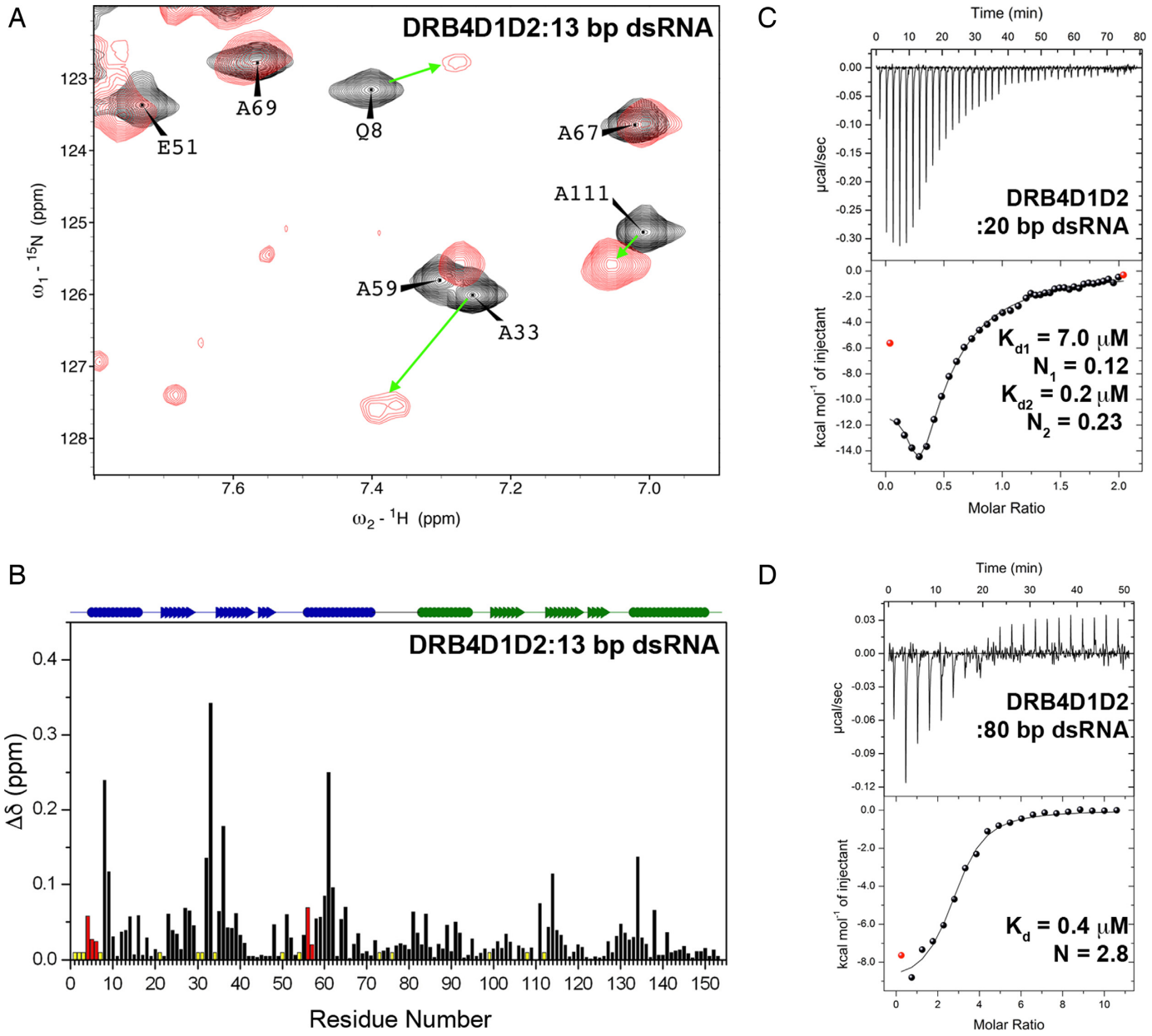

Figure 5. dsRNA binding studies on DRB4D1D2. (**A**) $^{1}H–^{15}N$ TROSY-HSQC excerpt of DRB4D1D2 (black) with 13 bp dsRNA (1:1.5 molar equivalence) (red). (**B**) Normalized chemical shift perturbations with 13 bp dsRNA mostly occur in dsRBD1. Red bars represent residues that undergo severe broadening whereas unassigned residues or proline are color coded in yellow. (**C**) ITC isotherms when fitted to two site sequential binding model to yield K_d corresponding to 7.3±0.6 μM and 0.2±0.1 μM. (**D**) One site binding model with 80 bp dsRNA, resulted in K_d of 0.4±0.03 μM. Red data points in ITC isotherms were omitted from data fitting.

can associate with four molecules of DRB4D1D2) and is higher than that of TRBPD1D2 and DRB1D1D2. TRBP and DRB1 were shown to associate with ∼20 bp dsRNA with 2:1 ratio (29,30). It appears that the shorter linker in DRB4D1D2 inhibits dsRBD2 from binding with the same dsRNA molecule leaving all four sites accessible for dsRBD1. Hence, the role of the linker in dsRNA binding needs to evaluated.

The NMR titrations between DRB4D1D2 and 20 bp dsRNA showed significant broadening for almost all resonances in DRB4D1D2 indicating that the dsRNA recognition mode of DRB4 dsRBDs with longer dsRNA is more complex (Supplementary Figure S9 and Supplementary Figure S10). Further analysis suggests that the α-helical dsRNA binding face in dsRBD1 is completely broadened, whereas remaining residues of dsRBD1, linker and dsRBD2 show broadening but were traceable. The broadening and the perturbation pattern in DRB4D1D2 strongly corroborate with the pattern observed for individual dsRBDs upon titration with 20 bp dsRNA.

The titration of DRB4D1D2 with 80 bp dsRNA resulted in the affinity constant of 0.4 μM with an averaged single site binding mode as the protein was titrated to dsRNA (Figure 5D and Supplementary Table S1). Similarly, DRB4

binds with 80 bp dsRNA yielding a K_d value of 0.12 μM (Supplementary Figure S11A and Supplementary Table S1). The ITC data also suggests that up to four dsRBDs bind to 20 bp dsRNA and the stoichiometry is more or less retained even in longer dsRNA (Supplementary Table S1).

Mutational studies reveal key RNA binding residues lie in dsRBD1

RNA binding property of residues from both dsRBDs was further validated by gel shift assays using several DRB4D1D2 single and double mutants in which amino acids from all three dsRNA binding regions were mutated (Figure 6A). For dsRBD1 mutations, only 30–40% dsRNA:dsRBP complex was formed. In contrast, 70–80% dsRNA bound complex were formed with the mutations in dsRBD2. A double mutant, one from each dsRBD, H32A/K133A, completely abrogated the dsRNA recognition by DRB4 as previously reported (19). Our study, however, establishes the importance of H32 over K133 in dsRNA binding. The result also signifies the importance of β1-β2 loop in dsRBD1 over its counterpart in dsRBD2, which was also evident from NMR titration studies (Figure 3B and E). It is important to note that double mutants in N-terminus of α2 (L56A/K57A and K133A/K134A) significantly affect the binding ability of DRB4D1D2, as evidenced by the absence of well-defined RNA bound complex in lane 5 and 8. Moreover, DRB4 double mutants showed the loss of RNA bound complex (Supplementary Figure S11B). Thus, results derived from mutagenesis study suggest that DRB4 has reduced affinity to dsRNA in the absence of active dsRBD1, which underlines significant role played by dsRBD1 in dsRNA recognition.

Linker attenuates dsRBD2 activity

We sought to know if the relative position of dsRBDs in tandem is vital for better dsRNA recognition as DRB4D1 and DRB4D2 are structurally identical. Toward this, we prepared a domain-swapped construct where dsRBD2 preceded to dsRBD1 (DRB4D2D1) and linker and N-terminal amino acids were kept intact.

DRB4D2D1 retained its ability to bind dsRNA using a single site binding mode, albeit with a lower affinity (∼1 μM), corresponding to DRB4D2 (Figures 1C and 6B). Titrations with 13 and 20 bp dsRNA resulted in chemical shift changes exclusively in dsRBD2 and were identical to DRB4D2 (Figures 6C, D and 3E). Surprisingly, dsRBD1 completely lost dsRNA affinity by its relocation to the second position, which might have resulted from its transient interactions with the linker or steric hindrance induced by the first domain. Further, DRB4LD1 and DRB4LD2, in which the linker precedes the dsRBD1 or dsRBD2, respectively, display a very low magnitude of Δδ, suggesting that the significant loss of dsRNA binding is due to the presence of linker at their N-terminus (Supplementary Figure S11C–F). These results are in strong favor of positional preference wherein dsRBD at the first position appears to be more accessible to dsRNA irrespective of the binding affinities. Moreover, spatial restrictions induced by the linker possibly modulate domain motions which may regulate dsRBD:dsRNA interaction in DRB4.

Relative orientation of domains is important for dsRNA binding

To explore if dsRBDs acquire a relatively preferred orientation, long-range distances (up to *ca*. 20 Å) were obtained using paramagnetic relaxation enhancement (PRE) studies. PREs resulting from A24C and A102C, where the nitroxyl radical was placed on the β sheet of dsRBD1 and dsRBD2, respectively, induce many intra-domain PREs but no inter-domain PREs (Supplementary Figure S12A). However, ample intra- and inter-domain PREs were observed when the spin label was charged on α helices of both dsRBDs (Q8C, A69C, N85C and M138C), indicating the maximum spatial separation between β sheets (>20 Å), while α helices from both domains are closer to each other (< 20 Å).

Further, we recalculated DRB4D1D2 structures with additional PRE derived distance restraints to explain the restricted accessibility of dsRBD2 to dsRNA. We observed that DRB4D1D2 folds into an extended conformation where both dsRBDs retain their fold while adopting a preferred domain orientation (Figure 7A). The quality of the PRE refined structures yielded Q_{PRE} values in the range 0.15–0.2. The ensemble backbone and sidechain RMSD of the structures were found to be 0.9 and 1.5 Å, respectively. Structures show that the linker connecting dsRBDs exhibit multiple conformations due to its flexible nature; however, the flexibility is restricted, as only nine amino acids constitute the linker. Surface representation did not reveal any close contacts for residues situated at the domain interface. In most of the conformations, the linker flanks α1 helix in dsRBD2 and may inhibit dsRBD2:dsRNA recognition. Thus, the structure provides the candid rationale for restricted accessibility of dsRBD2 to dsRNA. The PRE studies of DRB4D1D2 in the presence of 13 bp dsRNA yielded identical I_{para}/I_{dia} values, suggesting that the relative orientation of domains is retained in the presence of dsRNA (data not shown). As PREs also yield average distances like NOEs, the preferred orientation observed here is only an averaged conformation between the two domains.

We further independently validated DRB4D1D2 NMR derived structures by small angle X-ray scattering (SAXS) (Supplementary Figure S12B–D). Superposition of PRE refined NMR structures with the average SAXS envelope resulted in a normalized spatial discrepancy (NSD) in the range of 0.81–0.82, corroborating NMR-derived structures well with the SAXS surface envelope.

Previously reported interaction between DRB4D1 and DCL4-DUF283 (15) appear to be non-specific as our studies did not reveal any detectable levels of binding between DRB4D1D2 and DUF283 (Supplementary Figure S13A and B) suggesting that DRB4D1 is restricted only to dsRNA binding in *Arabidopsis* RNAi.

DISCUSSION

Plants depend on DRB4 in achieving efficient viral defense by two independent and spatially separated pathways i.e. *tasi*/siRNA mediated gene silencing (in the nucleus) and 'R' mediated antiviral response (in the cytoplasm). The study is driven to understand structural and mechanistic

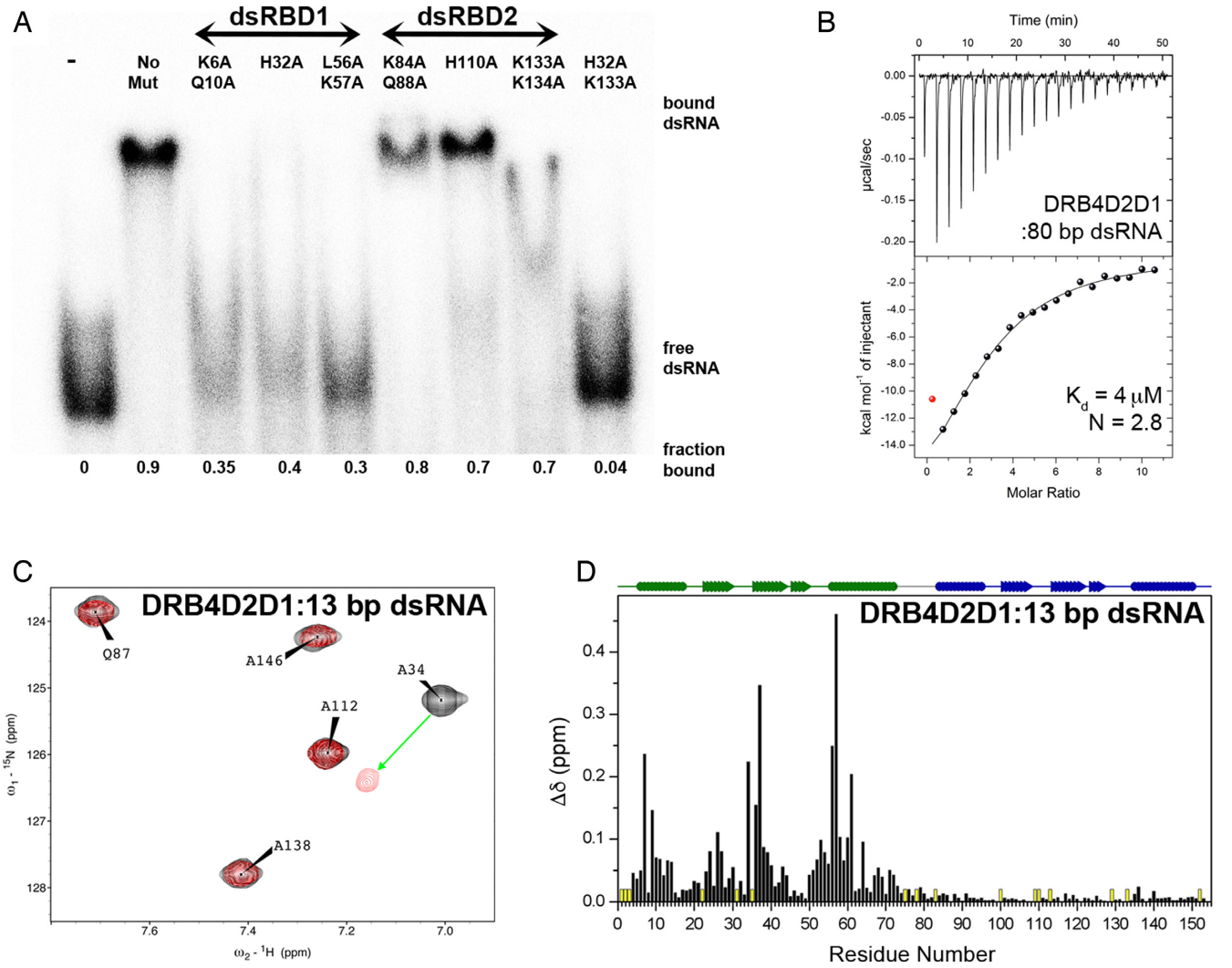

Figure 6. Mutagenesis and dsRNA binding with domain swapped construct. (**A**) Gel shift assay on the single and double mutants of DRB4D1D2 with 80 bp dsRNA. Mutant residues are annotated above respective lane. Mutations in key residues in dsRBD1 resulted in significant loss of dsRNA binding. (**B**) K_d derived from binding isotherm of DRB4D2D1 with 80 bp dsRNA is 4.0±0.4 µM ($N \approx 3$). (**C**) ^{1}H–^{15}N TROSY-HSQC excerpt of DRB4D2D1 with 13 bp dsRNA (black: blank, red: 1:2 (protein:dsRNA)). (**D**) Perturbations are observed only in dsRNA binding regions of dsRBD2. Unassigned residues and prolines are color coded in yellow.

details of specific roles exhibited by individual domains of DRB4 in the *tasi*/siRNA pathway.

The favorable structural arrangement and presence of dynamics at ms-µs timescale makes dsRBD1 as the domain of choice for the dsRNA interaction in DRB4. The low amplitude slow motions provide the necessary flexibility to the α1 helix in dsRBD1 so that it can be accommodated onto the minor groove of dsRNA. On the contrary, despite possessing a canonical dsRBD fold, dsRBD2 lacks the ideal sidechains orientation in the key RNA binding residues as well as the domain exhibits no significant motions. The work presented here highlights that the subtle structural differences along with the favorable dynamics in dsRBD1 influence dsRNA binding ability. The solution structure of DRB4D1D2 rationalizes the dsRNA binding results where preferential binding for dsRBD1 over dsRBD2 is seen. Residue specific interactions of DRB4D1D2 with dsRNA were quite unexpected, as the changes in chemical shifts for dsRBD2 were significantly reduced (∼30%) compared to the individual dsRBD2. Hence, the role of dsRBD2 in the *tasi*/siRNA pathway is unclear.

DRB4D1D2 structure suggests that conformations adopted by the linker possibly hinder the key dsRNA recognition amino acids in α1 of dsRBD2. In such scenario, dsRBD2:dsRNA complex formation is driven by contacts made only by the N-terminus of α2 and β1-β2 loop and would result in reduced binding. Further, the steric hindrance induced by the linker additionally reduces dsRNA recognition ability of DRB4D2. Therefore, we postulate that dsRBD2 may be recruited to recognize other RNA transcripts which does not require tripartite contact. Recently, in R protein mediated viral defense pathway, Jakubiec *et al.* have shown that DRB4D2, but not DRB4D1, binds to tRNA-like structure (TLS), which is a viral RNA translational enhancer and, therefore, may repress viral RNA translation (20). Therefore, we propose

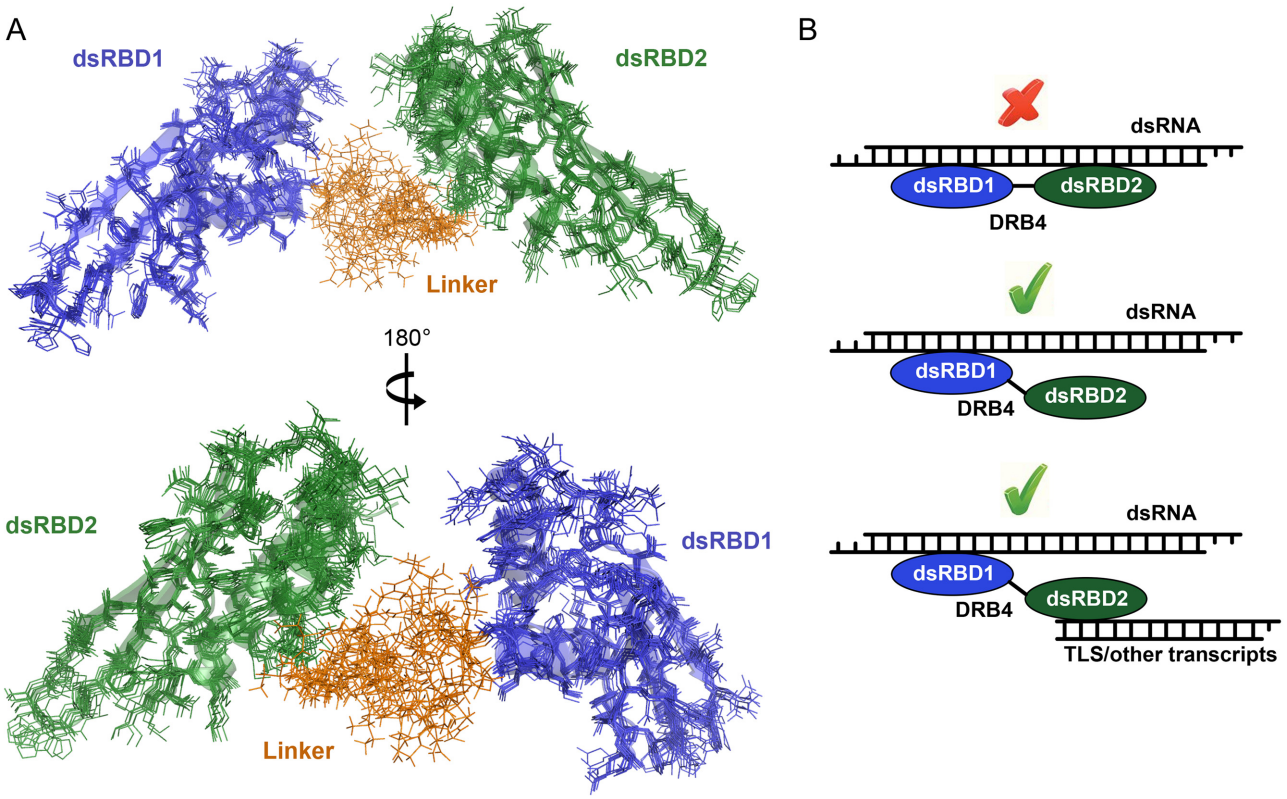

Figure 7. Structure and functional model of DRB4D1D2. (**A**) DRB4D1D2 adopt a preferred orientation. Ensemble of ten lowest energy PRE derived solution structures are represented as lines for dsRBD1 (blue) and dsRBD2 (green) and linker region (orange). The flexible linker connecting dsRBDs is situated on the opposite side of dsRNA recognition surface of dsRBD1. Linker residues sample conformations close to one of the dsRBD2 dsRNA binding site and hence may negatively affect its dsRNA binding ability. (**B**) DRB4D1 and DRB4D2 cannot simultaneously associate with the same molecule of dsRNA due to steric restriction imposed by short linker (top panel), however, high affinity of DRB4D1 and accessibility allows it to be the domain of choice for interaction with dsRNA (middle panel). The presence of linker reduces dsRNA binding affinity of DRB4D2 leading to its binding with other transcripts or tRNA like structures (TLS) (bottom panel).

that limited access of dsRBD2 to dsRNA may be an advantage for its strong association to viral tRNA-like structures, which contain stem loops and mismatches (Figure 7B).

One of the interesting features observed here is the linker's role in annihilating the function of the succeeding domain. Structure comparisons of DRB4D1D2 with DGCR8, where both dsRBDs assume a fixed orientation, suggest that DRB4 adopts a non-identical orientation implying an alternate dsRNA binding mechanism. We further explored binding of both dsRBDs to a single long dsRNA molecule, using a semi-experimental calculation (HADDOCK), which necessitates a minimum distance of ∼40 Å between the dsRBDs (data not shown). Assuming that nine amino acid long linker adopts an extended conformation, it can only span a maximum of 32 Å. Additionally, in order to achieve such binding, dsRBDs would adopt completely opposite orientation, similar to DGCR8, and contradict the PRE data. Hence, binding of both dsRBDs to a single dsRNA appears highly unrealistic (Figure 7B). The results suggest that the linker is not just a string connecting two domains but plays an important role in driving the substrate selection for both dsRBD.

Our study suggests that DRB4 dsRBDs use a complex mechanism to bind to longer dsRNA than previously studied dsRBPs such as TRBP and DRB1 (29,30). While a single dsRNA can associate with four molecules of individual and tandem dsRBDs, which is in agreement with TRBP (29), the presence of significant resonance broadening with DRB4D1 and DRB4D1D2 is perplexing. Previously, Benoit *et al*. observed only chemical shift perturbations and no broadening for TRBP12:mi155/pre-miR-155 titration perhaps due to the mismatches on miRNA which would not allow TRBP12 to slide over miRNA (28). In case of DRB4, the native trigger dsRNA for DRB4:DCL4 complex is always > 60 bp dsRNA with perfect palindromic sequence. Hence, like TRBP12 slides over a perfectly complimentary dsRNA (28), DRB4 dsRBD1 appears to have ability to slide over long dsRNA. As stated earlier, dsRBD1 is the principle dsRNA recognizer and the steric hindrance induced by the linker does not allow dsRBD2 to bind to the same molecule that is bound by dsRBD1. In this scenario, the complex formed by DRB4D1D2 with longer dsRNA will be highly heterogeneous and dynamic. The resonance broadening in NMR based titrations with 20 bp dsRNA is a result of multiple simultaneous events, i.e. binding of multiple dsRBD1 (up to four) with a single molecule of dsRNA, the binding kinetics, the sliding of dsRBD1 over the length of dsRNA and transient interactions of free dsRBD2 with another molecule of dsRNA. The mul-

tiple binding events and the sliding are also reflected in the broadening of imino protons of dsRNA and α-helical binding face in dsRBD1, whereas remaining residues of dsRBD1, linker and dsRBD2 experience broadening due to the formation of large macromolecular assembly. Given the complex nature of the binding, it is difficult to draw more definitive conclusion on the binding event of DRB4D1D2 with longer dsRNA.

The unstructured nature of PxxP motif rich DRB4C, its ability to bind to Zn^{2+} as well as the presence of a small structured domain at its C-terminus, allow us to propose its putative role in protein:protein and protein:membrane interaction. Recently, it was shown that the C-terminal regions of TRBP and PACT fold into a third dsRBD to mediate interaction with inter-Helicase PBD domain of Dicer (31). Interaction of Dicer with the C-terminal region of dsRBP appears as the universal feature because RNAi is an ancient and highly conserved gene regulatory pathway. As we identify a structured domain at the C-terminal region of DRB4 and assuming that DRB4Cc adopts a non-canonical dsRBD fold, for it has no sequence similarity to any dsRBD, we speculate that DRB4Cc may mediate DCL4 interaction. In addition to binding dsRNA, DRB4 is known to interact with several partner proteins in the RNAi pathway, like DCL4, SGS-3, DRB7 and also in viral defense pathway, like HRT and viral coat proteins. As PxxP motifs mediate protein-protein interaction and play a key role in signaling pathways (32), the presence of six PxxP motifs in DRB4C region, makes it an ideal candidate for interactions with HRT and other viral coat proteins. We assume that in other events, dsRBD1 would be in the free state, hence, inducing no steric hindrance on dsRBD2 which will be left free to bind other partners.

Our study elucidates that the key structural and dynamic features in dsRBD1 as well as the unique nature of the linker are important for the successful outcome of the tasi/siRNA pathway in plants.

DATA DEPOSITION

Solution structures for DRB4D1D2, DRB4D1 and DRB4D2 were deposited in RCSB protein databank with ID: 2N3F, 2N3G and 2N3H, respectively.

SUPPLEMENTARY DATA

Supplementary Data are available at NAR Online.

ACKNOWLEDGEMENTS

We acknowledge Prof. T. Fukuhara and Dr. Adam Yuan for the generous gift of recombinant pGEX6p-DRB4 and pET28b-DCL4-DUF283 plasmids, respectively and Dr. Sujoy Mukherjee (CSIR - IICB, Kolkata) for relaxation compensated CPMG pulse code. We also acknowledge N. Praveen Kumar, L. Madhurya, Puneeta Singh and K. Mallesham for general assistance. Additionally, we acknowledge Dr. B. Jagadeesh (CSIR-IICT, Hyderabad) for seamless access to 700 MHz spectrometer, Dr. Malay K. Ray and Dr. R. Sankaranarayanan for suggestions and discussion during the manuscript preparation, as well as Prof. Amitabha Chattopadhyay and Dr. B. Raman for help with control experiments.

Author contributions: M.D. planned the study and designed experiments. C.S.C., R.A., U.R. and M.D. performed experiments, interpreted results and wrote the paper.

FUNDING

CSIR network project GenCODE [BSC0123]; Council of Scientific and Industrial Research (CSIR) and University Grants Commission (UGC) [to C.S.C. and U.R.]. Funding for open access charge: CSIR network project GenCODE [BSC0123].

Conflict of interest statement. None declared.

REFERENCES

1. Hiraguri,A., Itoh,R., Kondo,N., Nomura,Y., Aizawa,D., Murai,Y., Koiwa,H., Seki,M., Shinozaki,K. and Fukuhara,T. (2005) Specific interactions between Dicer-like proteins and HYL1/DRB- family dsRNA-binding proteins in *Arabidopsis thaliana*. *Plant Mol. Biol.*, **57**, 173–188.
2. Bouche,N., Lauressergues,D., Gasciolli,V. and Vaucheret,H. (2006) An antagonistic function for Arabidopsis DCL2 in development and a new function for DCL4 in generating viral siRNAs. *EMBO J.*, **25**, 3347–3356.
3. Henderson,I.R., Zhang,X., Lu,C., Johnson,L., Meyers,B.C., Green,P.J. and Jacobsen,S.E. (2006) Dissecting *Arabidopsis thaliana* DICER function in small RNA processing, gene silencing, and DNA methylation patterning. *Nat. Genet.*, **38**, 721–725.
4. Mlotshwa,S., Pruss,G.J., Peragine,A., Endres,M.W., Li,J., Chen,X., Poethig,R.S., Bowman,L.H. and Vance,V. (2008) DICER-LIKE2 plays a primary role in transitive silencing of transgenes in Arabidopsis. *PLoS One*, **3**, e1755.
5. Liu,Q., Feng,Y. and Zhu,Z. (2009) Dicer-like (DCL) proteins in plants. *Funct. Integr. Genomics*, **9**, 277–286.
6. Xie,Z., Allen,E., Wilken,A. and Carrington,J.C. (2005) DICER-LIKE 4 functions in trans-acting small interfering RNA biogenesis and vegetative phase change in *Arabidopsis thaliana*. *Proc. Natl. Acad. Sci. U.S.A.*, **102**, 12984–12989.
7. Yoshikawa,M., Peragine,A., Mee,Y.P. and Poethig,R.S. (2005) A pathway for the biogenesis of trans-acting siRNAs in Arabidopsis. *Genes Dev.*, **19**, 2164–2175.
8. Blevins,T., Rajeswaran,R., Shivaprasad,P.V., Beknazariants,D., Si-Ammour,A., Park,H.S., Vazquez,F., Robertson,D., Meins,F., Hohn,T. *et al.* (2006) Four plant Dicers mediate viral small RNA biogenesis and DNA virus induced silencing. *Nucleic Acids Res.*, **34**, 6233–6246.
9. Deleris,A., Gallego-Bartolome,J., Bao,J., Kasschau,K.D., Carrington,J.C. and Voinnet,O. (2006) Hierarchical action and inhibition of plant Dicer-like proteins in antiviral defense. *Science*, **313**, 68–71.
10. Qu,F., Ye,X. and Morris,T.J. (2008) Arabidopsis DRB4, AGO1, AGO7, and RDR6 participate in a DCL4-initiated antiviral RNA silencing pathway negatively regulated by DCL1. *Proc. Natl. Acad. Sci. U.S.A.*, **105**, 14732–14737.
11. Adenot,X., Elmayan,T., Lauressergues,D., Boutet,S., Bouché,N., Gasciolli,V. and Vaucheret,H. (2006) DRB4-dependent TAS3 trans-acting siRNAs control leaf morphology through AGO7. *Curr. Biol.*, **16**, 927–932.
12. Nakazawa,Y., Hiraguri,A., Moriyama,H. and Fukuhara,T. (2007) The dsRNA-binding protein DRB4 interacts with the Dicer-like protein DCL4 in vivo and functions in the trans-acting siRNA pathway. *Plant Mol. Biol.*, **63**, 777–785.
13. Fukudome,A., Kanaya,A., Egami,M., Nakazawa,Y., Hiraguri,A., Moriyama,H. and Fukuhara,T. (2011) Specific requirement of DRB4, a dsRNA-binding protein, for the in vitro dsRNA-cleaving activity of Arabidopsis Dicer-like 4. *RNA*, **17**, 750–760.
14. Eamens,A.L., Smith,N.A., Curtin,S.J., Wang,M.-B. and Waterhouse,P.M. (2009) The *Arabidopsis thaliana* double-stranded

RNA binding protein DRB1 directs guide strand selection from microRNA duplexes. *RNA*, **15**, 2219–2235.
15. Qin,H., Chen,F., Huan,X., Machida,S., Song,J. and Yuan,Y.A. (2010) Structure of the *Arabidopsis thaliana* DCL4 DUF283 domain reveals a noncanonical double-stranded RNA-binding fold for protein-protein interaction. *RNA*, **16**, 474–481.
16. Kachroo,P., Chandra-Shekara,A.C. and Klessig,D.F. (2006) Plant signal transduction and defense against viral pathogens. *Adv. Virus Res.*, **65**, 161–191.
17. Zhu,S., Jeong,R.D., Lim,G.H., Yu,K., Wang,C., Chandra-Shekara,A.C., Navarre,D., Klessig,D.F., Kachroo,A. and Kachroo,P. (2013) Double-stranded RNA-binding protein 4 is required for resistance signaling against viral and bacterial pathogens. *Cell Rep*., **4**, 1168–1184.
18. Zhu,S., Lim,G., Yu,K., Jeong,R., Kachroo,A. and Kachroo,P. (2014) RNA silencing components mediate resistance signaling against turnip crinkle virus. *Plant Signal. Behav.*, **9**, e28435.
19. Haas,G., Azevedo,J., Moissiard,G., Geldreich,A., Himber,C., Bureau,M., Fukuhara,T., Keller,M. and Voinnet,O. (2008) Nuclear import of CaMV P6 is required for infection and suppression of the RNA silencing factor DRB4. *EMBO J*., **27**, 2102–2112.
20. Jakubiec,A., Yang,S.W. and Chua,N.H. (2012) Arabidopsis DRB4 protein in antiviral defense against Turnip yellow mosaic virus infection. *Plant J*., **69**, 14–25.
21. Montavon,T., Kwon,Y., Zimmermann,A., Hammann,P., Vincent,T., Cognat,V., Michel,F. and Dunoyer,P. (2017) A specific dsRNA-binding protein complex selectively sequesters endogenous inverted-repeat siRNA precursors and inhibits their processing. *Nucleic Acids Res*, **45**, 1330–1344.
22. Tschopp,M.A., Iki,T., Brosnan,C.A., Jullien,P.E. and Pumplin,N. (2017) A complex of Arabidopsis DRB proteins can impair dsRNA processing. *RNA*, **23**, 782–797.
23. Gleghorn,M.L. and Maquat,L.E. (2014) 'Black sheep' that don't leave the double-stranded RNA-binding domain fold. *Trends Biochem. Sci.*, **39**, 328–340.
24. Ryter,J.M. and Schultz,S.C. (1998) Molecular basis of double-stranded RNA-protein interactions: Structure of a dsRNA-binding domain complexed with dsRNA. *EMBO J*., **17**, 7505–7513.
25. Chiliveri,S.C. and Deshmukh,M.V. (2015) Chemical shift assignments of DRB4 (1-153), a dsRNA binding protein in *A. thaliana* RNAi pathway. *Biomol. NMR Assign.*, **9**, 253–256.
26. Romero,P., Obradovic,Z., Li,X., Garner,E.C., Brown,C.J. and Dunker,A.K. (2001) Sequence complexity of disordered protein. *Proteins Struct. Funct. Genet.*, **42**, 38–48.
27. Stefl,R., Oberstrass,F.C., Hood,J.L., Jourdan,M., Zimmermann,M., Skrisovska,L., Maris,C., Peng,L., Hofr,C., Emeson,R.B. *et al.* (2010) The solution structure of the ADAR2 dsRBM-RNA complex reveals a sequence-specific readout of the minor groove. *Cell*, **143**, 225–237.
28. Koh,H.R., Kidwell,M.A., Ragunathan,K., Doudna,J.A. and Myong,S. (2013) ATP-independent diffusion of double-stranded RNA binding proteins. *Proc. Natl. Acad. Sci. U.S.A.*, **110**, 151–156.
29. Benoit,M.P., Imbert,L., Palencia,A., Perard,J., Ebel,C., Boisbouvier,J. and Plevin,M.J. (2013) The RNA-binding region of human TRBP interacts with microRNA precursors through two independent domains. *Nucleic Acids Res.*, **41**, 4241–4252.
30. Yang,S.W., Chen,H.Y., Yang,J., Machida,S., Chua,N.H. and Yuan,Y.A. (2010) Structure of Arabidopsis HYPONASTIC LEAVES1 and its molecular implications for miRNA processing. *Structure*, **18**, 594–605.
31. Heyam,A., Lagos,D. and Plevin,M. (2015) Dissecting the roles of TRBP and PACT in double-stranded RNA recognition and processing of noncoding RNAs. *Wiley Interdiscip. Rev. RNA*, **6**, 271–289.
32. Chandra,B.R., Gowthaman,R., Akhouri,R.R., Gupta,D. and Sharma,A. (2004) Distribution of proline- rich (PxxP) motifs in distinct proteomes: Functional and therapeutic implications for malaria and tuberculosis. *Protein Eng. Des. Sel.*, **17**, 175–182.